Structural Engineering and Mechanics, *Vol. 69, No. 2 (2019) 231-241*
DOI: https://doi.org/10.12989/sem.2019.69.2.231

An analytical solution for bending and free vibration responses of functionally graded beams with porosities: Effect of the micromechanical models

Lazreg Hadji*[1,3], Nafissa Zouatnia[2,3] and Fabrice Bernard[4]

[1]*Laboratory of Geomatics and Sustainable Development, Ibn Khaldoun University of Tiaret, Algeria*
[2]*Department of Civil Engineering, Laboratory of Structures, Geotechnics and Risks (LSGR), Hassiba Benbouali University of Chlef, BP 151, Hay Essalam, UHB Chlef, Chlef (02000), Algeria*
[3]*Department of Civil Engineering, Ibn Khaldoun University, BP 78 Zaaroura, 14000 Tiaret, Algeria*
[4]*University of Rennes, INSA Rennes, Laboratory of Civil Engineering and Mechanical Engineering, France*

(Received October 16, 2018, Revised December 14, 2018, Accepted December 15, 2018)

Abstract. In this paper, a new higher order shear deformation model is developed for static and free vibration analysis of functionally graded beams with considering porosities that may possibly occur inside the functionally graded materials (FGMs) during their fabrication. Different patterns of porosity distributions (including even and uneven distribution patterns, and the logarithmic-uneven pattern) are considered. In addition, the effect of different micromechanical models on the bending and free vibration response of these beams is studied. Various micromechanical models are used to evaluate the mechanical characteristics of the FG beams whose properties vary continuously across the thickness according to a simple power law. Based on the present higher-order shear deformation model, the equations of motion are derived from Hamilton's principle. Navier type solution method was used to obtain displacement, stresses and frequencies, and the numerical results are compared with those available in the literature. A comprehensive parametric study is carried out to assess the effects of volume fraction index, porosity fraction index, micromechanical models, mode numbers, and geometry on the bending and natural frequencies of imperfect FG beams.

Keywords: functionally graded materials; bending; free vibration; micromechanical models; porosity

1. Introduction

Functionally graded materials (FGMs) are advanced composite materials made of two or more constituent phases. The concept of FGM was first considered in Japan in 1984 during a space plane project. The FGM materials can be designed for specific applications. For example, thermal barrier coatings for turbine blades (electricity production), armor protection for military applications, fusion energy devices, biomedical materials including bone and dental implants, space/aerospace industries, automotive applications, etc. Several studies have been performed to analyze the mechanical responses of FG structures. Belabed *et al.* 2014 used an efficient and simple higher order shear and normal deformation theory for functionally graded material (FGM) plates. Hebali *et al.* (2014) investigated a new quasi-3D hyperbolic shear deformation theory for the static and free vibration analysis of functionally graded plates. Ait Amar Meziane *et al.* (2014) studied the buckling and free vibration of exponentially graded sandwich plates under various boundary conditions using an efficient and simple refined theory. Hamidi *et al.* (2015) studied the thermomechanical bending of functionally graded sandwich plates using a sinusoidal plate theory with 5-unknowns and stretching effect. Mahi *et al.* (2015) used a new hyperbolic shear deformation theory for bending and free vibration analysis of isotropic, functionally graded, sandwich and laminated composite plates. Akbaş *et al.* (2015a) studied the wave propagation of a functionally graded beam in thermal environments. Akbaş *et al.* (2015b) developed the post-buckling behavior of edge cracked functionally graded beams under axial loads. Akbaş *et al.* (2015c) analyze the post-buckling of axially functionally graded three-dimensional beams.

Nowadays, functionally graded beams and plates structures are widely used in many industries including nuclear engineering. Therefore, accurate structural analysis of FG beams is required to predict their correct bending, and vibration behavior. Also, it is grasped that in the process of FGM manufacturing, microvoids (known as porosities) can take place within the materials during the sintering action (Zhu *et al.* 2001). This phenomenon is related to the large difference in solidification temperatures between material components (Wang *et al.* 2017). Due to the importance of this subject, several studies have been carried out to explore the porosity effects. For example, Ait Atmane *et al.* (2015) studied the free vibration of microbeams made of porous graded materials using a higher order shear deformation theory. Gupta and Talha (2017) examined the effect of porosity on the frequency response of FG plates in the presence of a thermal effect by using a non-polynomial higher-order shear and normal deformation theory. Akbaş *et al.* (2017a) analyze the nonlinear static of functionally graded porous beams under thermal effect. Akbaş *et al.*

*Corresponding author, Ph.D.
E-mail: had_laz@yahoo.fr

ISSN: 1225-4568 (Print), 1598-6217 (Online)

(2017b) studied the post-buckling responses of functionally graded beams with porosities. Akbaş *et al.* (2017c) studied the thermal effects on the vibration of functionally graded deep beams with porosity. Akbaş *et al.* (2017d) analyze the vibration and static analysis of functionally graded porous plates. Akbaş *et al.* (2018a) analyze the forced vibration of functionally graded porous deep beams. Akbaş *et al.* (2018b) investigated the geometrically nonlinear of functionally graded porous beams.

In order to model FGM precisely, it is essential to know the effective or bulk material properties as a function of individual material properties and geometry, in particular at micromechanics level.

In recent years, different models have been proposed to estimate the effective properties of FGMs with respect to reinforcement volume fractions (Shen and Wang 2012, Jha *et al.* 2013). Consequently, several micromechanical models have been used to study and analyze the behavior of FGM structures under different loading conditions. We cite as an example the work of Gasik (1998) in which a micromechanical model is proposed to study FGMs with a random distribution of constituents. The FGM microstructures were idealized by homogeneous materials (sub-cells) with cubic inclusions. Each substring corresponded to a fixed volume. Thereafter, the elastic constants as well as the coefficient of thermal expansion calculated from this model were compared with those obtained from the Mori-Tanaka Voigt, and Kerner's models. Using an appropriate micromechanical model, Yin *et al.* (2004) and Yin *et al.* (2007) have determined the expressions of the linear coefficient of thermal expansion, the Young's moduli and the Poisson's ratio.

In the present study, static and free vibration of simply supported FG beams was investigated by using new higher order Shear Deformation model. Different patterns of porosity distributions (including even and uneven distribution patterns, and the logarithmic-uneven pattern) are considered. In addition, the effect of different micromechanical models on the bending and free vibration response of these beams is studied. Various micromechanical models are used to evaluate the mechanical characteristics of the FG beams whose properties vary continuously across the thickness according to a simple power law. Then, the present model together with Hamilton's principle, are employed to extract the motion equations of the functionally graded beams. Analytical solutions for static and free vibration are obtained. The effects of various variables, such as span-to-depth ratio, gradient index, the volume fraction of porosity and micromechanical models on bending and free vibration of FG beam are all discussed.

2. Effective properties of FGMs

Unlike traditional microstructures, in FGMs the material properties are spatially varying, which is not trivial for a micromechanics model (Jaesang and Addis 2014).

A number of micromechanics models have been proposed for the determination of effective properties of FGMs. In what follows, we present some micromechanical models to calculate the effective properties of the FG beam.

2.1 Voigt model

The Voigt model is relatively simple; this model is frequently used in most FGM analyses that estimates Young's modulus E of FGMs as (Mishnaevsky 2007)

$$E(z) = E_c \mathrm{V_c} + E_m\left(1 - V_c\right) \tag{1}$$

2.2 Reuss model

The Voigt model is relatively simple; this model is frequently used in most FGM analyses estimates Young's modulus E of FGMs as (Mishnaevsky 2007)

$$E(z) = \frac{E_c E_m}{E_c\left(1 - V_c\right) + E_m V_c} \tag{2}$$

2.3 Tamura model

The Tamura model uses actually a linear rule of mixtures, introducing one empirical fitting parameter known as "stress-to-strain transfer" (Gasik 1995)

$$q = \frac{\sigma_1 - \sigma_2}{\varepsilon_1 - \varepsilon_2} \tag{3}$$

Estimate for q=0 correspond to Reuss rule and with q=100 to the Voigt rule, being invariant to the consideration of with phase is matrix and which is particulate. The effective Young's modulus is found as

$$E(z) = \frac{\left(1 - V_c\right)E_m\left(q - E_c\right) + V_c E_c\left(q - E_m\right)}{\left(1 - V_c\right)\left(q - E_c\right) + V_c E_c\left(q - E_m\right)} \tag{4}$$

2.4 Description by a representative volume element (LRVE)

The local representative volume element (LRVE) is based on a "mesoscopic" length scale which is much larger than the characteristic length scale of particles (inhomogeneities) but smaller than the characteristic length scale of a macroscopic specimen (Ju and Chen 1994). The LRVE is developed based on the assumption that the microstructure of the heterogeneous material is known. The input for the LRVE for the deterministic micromechanical framework is usually volume average or ensemble average of the descriptors of the microstructures.

Young's modulus is expressed as follows by the LRVE method (Akbarzadeh *et al.* 2015)

$$E(z) = E_m\left(1 + \frac{V_c}{FE - \sqrt[3]{V_c}}\right),\ FE = \frac{1}{1 - \frac{E_m}{E_c}} \tag{5}$$

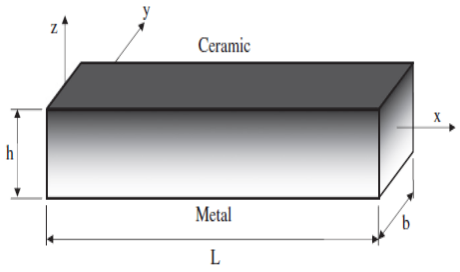

Fig. 1 Geometry and coordinate of a FG beam

2.5 Mori-Tanaka model

The locally effective material properties can be provided by micromechanical models such as the Mori-Tanaka estimates. This method based on the assumption that a two-phase composite material consisting of matrix reinforced by spherical particles, randomly distributed in the plate. According to Mori-Tanaka homogenization scheme, the Young's modulus is given as

$$E(z) = E_m + (E_c - E_m)\left(\frac{V_c}{1+(1-V_c)(E_c/E_m-1)(1+\nu)/(3-3\nu)}\right) \quad (6)$$

where $V_c = \left(\frac{1}{2}+\frac{z}{h}\right)^p$ is the volume fraction of the ceramic and where p is the power law index. Since the effects of the variation of Poisson's ratio (ν) on the response of FGM plates are very small (Kitipornchai 2006), this material parameter is assumed to be constant for convenience.

3. Preliminary concepts and definitions

Consider a functionally graded beam with length L and rectangular cross section b×h, with b being the width and h being the height as shown in Fig. 1. The beam is made of isotropic material with material properties varying smoothly in the thickness direction.

Beam's material is made from metal with a volume fraction $V_m(z)$ and from ceramic with a volume fraction $V_c(z)$. The volume fraction of ingredient materials is distributed as the equations below

$$V_c(z) = \left(\frac{z}{h}+\frac{1}{2}\right)^p, \; V_m(z) = 1 - V_c(z), \quad (7)$$

Where p is volume fraction index $0 \le p \le \infty$. In case p=0, the beam is made entirely from ceramic. When p=∞ the beam made completely from metal. Coefficient p defines the material distribution of the structure.

The characteristic of material made beams are written

$$P(z) = (P_c - P_m)\left(\frac{z}{h}+\frac{1}{2}\right)^p + P_m - P_{por} \quad (8)$$

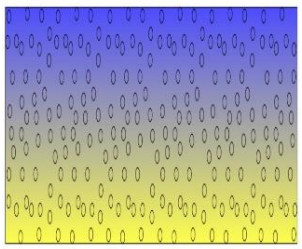

(a)

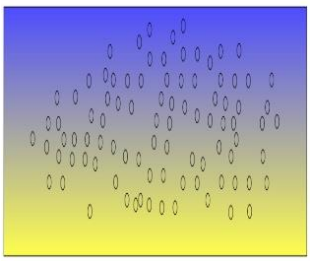

(b)

Fig. 2 Porosity models: (a) Evenly distributed porosities, (b) Unevenly distributed porosities

In this study, four types of porosity are considered, some of them present an evenly distribution (called hereafter Imperfect I and III), whereas the other ones are characterized by an unevenly distribution (Imperfect II and IV hereafter), along the beam thickness direction (Fig. 2).

The various expressions of the porosity distribution are presented in the following equations

The porosity is distributed as equations below.

- Imperfect-I

$$P_{por} = \frac{\alpha}{2}(P_c + P_m) \quad (9)$$

- Imperfect II

$$P_{por} = \frac{\alpha}{2}\left(1-\frac{2|z|}{h}\right)(P_c + P_m) \quad (10)$$

- Imperfect III

$$P(z) = \left((P_c - P_m)\left(\frac{z}{h}+\frac{1}{2}\right)^p + P_m\right)(1-\alpha)^3 \quad (11)$$

- Imperfect IV

Imperfect III and IV models are an adaptation of widely used expressions for cement-based materials (Kendall *et al.* 2003).

$$P(z) = \left((P_c - P_m)\left(\frac{z}{h}+\frac{1}{2}\right)^p + P_m\right)\left(1-\alpha\left(1-2\frac{|z|}{h}\right)\right)^3 \quad (12)$$

The material properties of FGM porous beam such as the elastic modulus E, the thermal expansion coefficient β, and mass density ρ can be written, for the various porosity distribution models, as follows

Imperfect-I

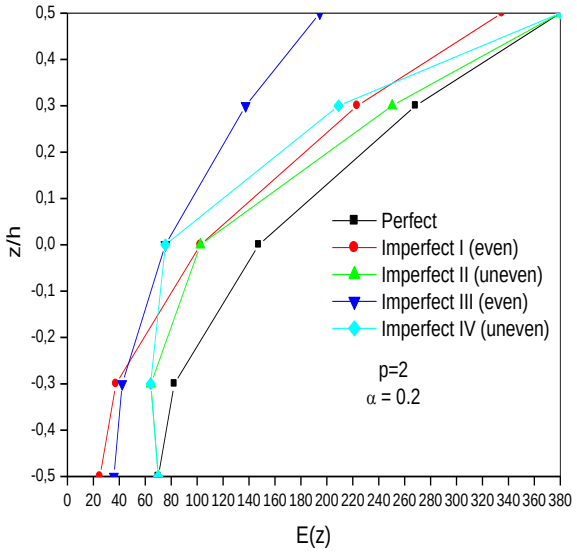

Fig. 3 Variation of the fundamental frequency $\bar{\omega}$ of embedded perfect and imperfect FG beams (p=2) versus L/h ratio (α=0.2)

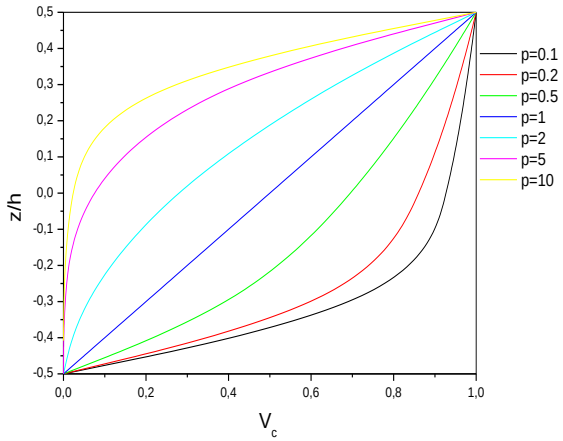

Fig. 4 Variation of volume fraction V_c through the thickness of FG beam for various values of power law index p

$$\begin{bmatrix} E(z) \\ \beta(z) \\ \rho(z) \end{bmatrix} = \begin{bmatrix} E_{cm} \\ \beta_{cm} \\ \rho_{cm} \end{bmatrix} \left(\frac{z}{h} + \frac{1}{2} \right)^{p} + \begin{bmatrix} E_m \\ \beta_m \\ \rho_m \end{bmatrix} - \frac{\alpha}{2} \begin{bmatrix} E_c + E_m \\ \beta_c + \beta_m \\ \rho_c + \rho_m \end{bmatrix} \tag{13a}$$

Imperfect-II

$$\begin{bmatrix} E(z) \\ \beta(z) \\ \rho(z) \end{bmatrix} = \begin{bmatrix} E_{cm} \\ \beta_{cm} \\ \rho_{cm} \end{bmatrix} \left(\frac{z}{h} + \frac{1}{2} \right)^{p} + \begin{bmatrix} E_m \\ \beta_m \\ \rho_m \end{bmatrix} - \frac{\alpha}{2} \left(1 - 2\frac{|z|}{h} \right) \begin{bmatrix} E_c + E_m \\ \beta_c + \beta_m \\ \rho_c + \rho_m \end{bmatrix} \tag{13b}$$

Imperfect-III

$$\begin{bmatrix} E(z) \\ \beta(z) \\ \rho(z) \end{bmatrix} = \left(\begin{bmatrix} E_{cm} \\ \beta_{cm} \\ \rho_{cm} \end{bmatrix} \left(\frac{z}{h} + \frac{1}{2} \right)^{p} + \begin{bmatrix} E_m \\ \beta_m \\ \rho_m \end{bmatrix} \right) (1 - \alpha)^3 \tag{13c}$$

Imperfect-IV

$$\begin{bmatrix} E(z) \\ \beta(z) \\ \rho(z) \end{bmatrix} = \left(\begin{bmatrix} E_{cm} \\ \beta_{cm} \\ \rho_{cm} \end{bmatrix} \left(\frac{z}{h} + \frac{1}{2} \right)^{p} + \begin{bmatrix} E_m \\ \beta_m \\ \rho_m \end{bmatrix} \right) \left(1 - \alpha \left(1 - 2\frac{|z|}{h} \right) \right)^3 \tag{13d}$$

Where $E_{cm}=E_c-E_m$, $\beta_{cm}=\beta_c-\beta_m$, $\rho_{cm}=\rho_c-\rho_m$ and the Poisson ratio $v(z)$ is assumed to be constant $v(z)=v$.

Fig. 3 illustrates the variation of Young's modulus $E(z)$ through the thickness of embedded perfect and imperfect FG beams at a constant value of power law index (p=2).

2.2 New higher order shear deformation model for functionally graded beams

The assumed displacement field is as follows

$$u(x,z,t) = u_0(x,t) - z\frac{\partial w_0}{\partial x} + \frac{1}{\lambda_x}\left[\frac{3}{2}\left(\frac{z}{h} \right) - 2\left(\frac{z}{h} \right)^3 \right] Q_x \tag{14a}$$

$$w(x,z,t) = w_0(x,t) \tag{14b}$$

Where u_0 is displacements at any point (x, 0) on the reference plane in the x direction. Q_x is the transverse shear stress resultant with λ_x being the unknown constants. The constant λ_x can be determined by considering the definition of Q_x

$$Q_x = \int_{-h/2}^{h/2} \tau_{xz}\, dz \tag{15}$$

The strains associated with the displacements in Eq. (14) are

$$\varepsilon_x = \frac{\partial u_0}{\partial x} - z\frac{\partial^2 w}{\partial x^2} + \frac{1}{\lambda_x}\left[\frac{3}{2}\left(\frac{z}{h} \right) - 2\left(\frac{z}{h} \right)^3 \right] \frac{\partial Q_x}{\partial x} \tag{16a}$$

$$\gamma_{xz} = \frac{1}{\lambda_x}\left[\frac{3}{2h} - \frac{6z^2}{h^3} \right] Q_x \tag{16b}$$

The material properties (E; G; ρ) of Al/Al_2O_3 FG beam are supposed to vary continuously in the thickness direction according to power law (P-FGM) and exponential law (E-FGM) distributions. However, as commonly considered for simplicity, Poisson's ratio (v) of the beam is assumed to be constant through the thickness.

– The power law (P-FGM)

$$E(z) = (E_c - E_m)\left(\frac{z}{h} + \frac{1}{2} \right)^{p} + E_m \tag{17a}$$

$$\rho(z) = (\rho_c - \rho_m)\left(\frac{z}{h} + \frac{1}{2} \right)^{p} + \rho_m \tag{17b}$$

– The exponential law (E-FGM)

$$E(z)=E_m\exp\left[\log\left(\frac{E_c}{E_m}\right)\left(\frac{z}{h}+\frac{1}{2}\right)\right] \tag{18a}$$

$$\rho(z)=\upsilon_m\exp\left[\log\left(\frac{\rho_c}{\rho_m}\right)\left(\frac{z}{h}+\frac{1}{2}\right)\right] \tag{18b}$$

In these expressions, subscripts *m* and *c* represent the metallic and ceramic constituents, respectively; and *p* is the power law index. *z*/*h* is the thickness coordinate. A value of *p* equal to zero represents a fully ceramic beam, whereas infinite *p* indicates a fully metallic beam. The variation of the combination of ceramic and metal is linear for *p*=1 and non-linear for *p*=2, 5, 10, etc. Fig. 4 illustrates the variation of the volume fraction V_c through the thickness of the beam for various values of the power law index. The stress-strain relationship at any point in the beam is given by the one-dimensional Hooke's law as follows

$$\sigma_x=Q_{11}(z)\,\varepsilon_x \text{ and } \tau_{xz}=Q_{55}(z)\,\gamma_{xz} \tag{19}$$

Where

$$Q_{11}(z)=E(z) \text{ and } \mathrm{Q_{55}(z)}=\frac{\mathrm{E(z)}}{2(1+\nu)} \tag{20}$$

Using Eq. (16b) in the constitutive relations for τ_{xz} and then substituting in the Eq. (15) λ_x may be obtained as follows

$$\lambda_x=\frac{E(z)}{2(1+\nu)} \tag{21}$$

2.3 Equations of motion

The equations of motion are obtained using the principle of variational energy and virtual work.

$$\frac{\partial \mathrm{N_x}}{\partial \mathrm{x}}=\mathrm{I}_0\frac{\partial^2 \mathrm{u}_0}{\partial \mathrm{t}^2}-\mathrm{I}_1\frac{\partial^3 \mathrm{w}_0}{\partial \mathrm{x}\partial \mathrm{t}^2}+\frac{\mathrm{I}_8}{\lambda_\mathrm{x}}\frac{\partial^2 \mathrm{Q_x}}{\partial \mathrm{t}^2} \tag{22a}$$

$$\frac{\partial^2 M_x}{\partial x^2}=-q+I_0\frac{\partial^2 w_0}{\partial t^2}+I_1\frac{\partial^3 u_0}{\partial x\partial t^2}-I_2\frac{\partial^4 w_0}{\partial x^2\partial t^2}+I_9\left(\frac{1}{\lambda_x}\frac{\partial^3 Q_x}{\partial x\partial t^2}\right) \tag{22b}$$

$$\frac{\partial}{\partial x}\left[M_x-\frac{4}{3h^2}P_x\right]-\left[Q_x-\frac{4}{h^2}R_x\right]=\frac{I_8}{\lambda_x}\frac{\partial^2 u_0}{\partial t^2}-\frac{I_9}{\lambda_x}\frac{\partial^3 w_0}{\partial x\partial t^2}+\frac{I_7}{\lambda_x^{\,2}}\frac{\partial^2 Q_x}{\partial t^2} \tag{22c}$$

The stress resultants and moment resultants are given by

$$(N_x,M_x,P_x)=\int_{-h/2}^{h/2}\sigma_x\left(1,z,z^3\right)dz \tag{23a}$$

$$R_x=\int_{-h/2}^{h/2}z^2\tau_{xz}\,dz \tag{23b}$$

The various stiffness parameters are defined as follows

$$(A_{11},B_{11},D_{11},E_{11},F_{11},H_{11})=\int_{-h/2}^{h/2}Q_{11}(z)\left(1,z,z^2,z^3,z^4,z^6\right)dz \tag{24a}$$

$$\left(A_{55},D_{55},F_{55}\right)=\int_{-h/2}^{h/2}Q_{55}(z)\left(1,z^2,z^4\right)dz \tag{24b}$$

The mass parameters are defined by

$$(\mathrm{I_0,I_1,I_2,I_3,I_4,I_6})=\int_{-\mathrm{h}/2}^{\mathrm{h}/2}\rho(\mathrm{z})\left(1,\mathrm{z},\mathrm{z}^2,\mathrm{z}^3,\mathrm{z}^4,\mathrm{z}^6\right)\mathrm{dz} \tag{25a}$$

$$\begin{aligned}&\mathrm{I_7}=\frac{9}{4\mathrm{h}^2}\mathrm{I_2}-\frac{6}{\mathrm{h}^4}\mathrm{I_4}+\frac{4}{\mathrm{h}^6}\mathrm{I_6};\\ &\mathrm{I_8}=\frac{3}{2\mathrm{h}}\mathrm{I_1}-\frac{2}{\mathrm{h}^3}\mathrm{I_3}\ \text{ and }\ \mathrm{I_9}=\frac{3}{2\mathrm{h}}\mathrm{I_2}-\frac{2}{\mathrm{h}^3}\mathrm{I_4}\end{aligned} \tag{25b}$$

3. Analytical solution

The equations of motion admit the Navier solutions for simply supported beams. The variables u_0, w_0, Q_x can be written by assuming the following variations

$$u_0=\sum_{m=1}^{\infty}U_m\cos\frac{m\pi x}{x}e^{-i\omega t} \tag{26a}$$

$$w_0=\sum_{m=1}^{\infty}W_m\sin\frac{m\pi x}{L}e^{-i\omega t} \tag{26b}$$

$$Q_x=\sum_{m=1}^{\infty}Q_{xm}\cos\frac{m\pi x}{L}e^{-i\omega t} \tag{26c}$$

where ω is the natural frequency. For the flexural analysis the term $e^{-i\omega t}$ is absent in the above expressions. Further, the transverse load *q* is also expanded in Fourier series as

$$q(x)=\sum_{m=1}^{\infty}Q_m\sin(\lambda x) \tag{27}$$

where Q_m is the load amplitude calculated from

$$Q_m=\frac{2}{L}\int_0^L q(x)\sin(\lambda x)dx \tag{28}$$

The coefficients Q_m are given below for some typical loads.

$$Q_m=q_0 \quad \text{Sinusoidal load} \tag{29a}$$

$$Q_m=\frac{4q_0}{m\pi} \quad \text{Uniform load} \tag{29b}$$

Table 1 Non-dimensional deflection of functionally graded (P-FGM) beam

L/h	p	Theory	Uniform load	Sinusoidal load
5	0 (ceramic)	Sayyad *et al.* (2018)	3.1635	2.5004
		Present	3.1654	2.5019
	1	Sayyad *et al.* (2018)	6.2563	4.9432
		Present	6.2594	4.9457
	2	Sayyad *et al.* (2018)	8.0666	6.3745
		Present	8.0677	6.3754
	5	Sayyad *et al.* (2018)	9.8414	7.7830
		Present	9.8281	7.7723
	10	Sayyad *et al.* (2018)	10.940	8.6547
		Present	10.9381	8.6530
	∞ (metal)	Sayyad *et al.* (2018)	17.173	13.574
		Present	17.183	13.582
10	0 (ceramic)	Sayyad *et al.* (2018)	2.9496	2.3271
		Present	2.9501	2.3275
	1	Sayyad *et al.* (2018)	5.8951	4.6506
		Present	5.8959	4.6512
	2	Sayyad *et al.* (2018)	7.5671	5.9698
		Present	7.5673	5.9699
	3	Sayyad *et al.* (2018)	9.0238	7.1207
		Present	9.0204	7.1179
	10	Sayyad *et al.* (2018)	9.9411	7.8452
		Present	9.9403	7.8446
	∞ (metal)	Sayyad *et al.* (2018)	16.012	12.633
		Present	16.015	12.635
100	0 (ceramic)	Sayyad *et al.* (2018)	2.8790	2.2699
		Present	2.8790	2.2699
	1	Sayyad *et al.* (2018)	5.7758	4.5538
		Present	5.7758	4.5538
	2	Sayyad *et al.* (2018)	7.4020	5.8359
		Present	7.4019	5.8359
	5	Sayyad *et al.* (2018)	8.7535	6.9016
		Present	8.7534	6.9015
	10	Sayyad *et al.* (2018)	9.6105	7.5773
		Present	9.6105	7.5773
	∞ (metal)	Sayyad *et al.* (2018)	15.628	12.322
		Present	15.628	12.322

Eqs. (26) and (27) reduce the governing equations to the following form

For flexural analysis

$$[C]\{\Delta\}=\{f\} \tag{30a}$$

and for free vibration analysis

$$\left([C]-\omega^2[G]\right)\{\Delta\}=0 \tag{30b}$$

$\{\Delta\}^{\mathrm{T}}=\{\mathrm{U_m},\mathrm{W_m},\mathrm{Q_{xm}}\}$ and $\{\mathrm{f}\}^{\mathrm{T}}=\{0,\mathrm{Q_m},0\}$

Where $[C]$ and $[G]$ refers to the flexural stiffness and mass matrices and ω to the corresponding frequency.

4. Results and discussion

In this study, bending, and free vibration analysis of simply supported perfect and imperfect FG beams is suggested for investigation. The FG beams are made of aluminium (Al;E_m=70 Gpa, ν_m=0.3, ρ_m=2702 kg/m^3 and alumina (Al_2O_3; E_c=380 Gpa, ν_c=0.3, ρ_c=3960 kg/m^3) and their properties change through the thickness of the beam according to a power or an exponential law.

For a sake of simplicity the displacements, stresses, and natural frequencies are presented in a non-dimensional form

$$\begin{gathered}\bar{w}=100\frac{E_m h^3}{q_0 L^4}w\left(\frac{L}{2}\right),\\ \bar{u}=100\frac{E_m h^3}{q_0 L^4}u\left(0,-\frac{h}{2}\right),\\ \bar{\sigma}_x=\frac{h}{q_0 L}\sigma_x\left(\frac{L}{2},\frac{h}{2}\right),\ \bar{\tau}_{xz}=\frac{h}{q_0 L}\tau_{xz}(0,0),\\ \bar{\omega}=\frac{\omega L^2}{h}\sqrt{\frac{\rho_m}{E_m}}\end{gathered} \tag{31}$$

Study 1 Bending analysis of simply supported functionally graded (P-FGM) and exponentially graded (EFGM) beams.

For the bending analysis, the beam is made of FG material and its properties vary through the thickness of the beam according to the power law (P-FGM) and exponential law (E-FGM) distributions. The beam is subjected to uniform and sinusoidal transverse loads in z-direction. The axial displacement, transverse displacement, axial stress, and the transverse shear stress are non-dimensionalised using Eq. (31). Table 1 shows the nondimensional displacements of FG beams subjected to uniform and sinusoidal load for different values of power law index p and span-to-depth ratio L/h. The results obtained are compared with the results of the exponential shear deformation theory (ESDBT) developed by Sayyad *et al.* (2018). It can be observed that the present results are in an excellent agreement with those predicted using the shear deformation beam theory developed by Sayyad *et al.* (2018). In Table 2, maximum nondimensional displacements and stresses of the P-FGM beam are presented for various values of the power law index p and a span-to-depth ratio L/h=5. For the comparison purpose, the numerical results for a simply supported FG beam using

Table 2 Non-dimensional displacements and stresses of functionally graded (P-FGM) beams (L=5h)

p	Theory	Model	Uniform load			Sinusoidal load		
			$\bar{w}$	$\bar{\sigma}_x$	$\bar{\tau}_{xz}$	$\bar{w}$	$\bar{\sigma}_x$	$\bar{\tau}_{xz}$
0	Present	ZSDBT	3.1654	3.8019	0.7329	2.5020	3.0916	0.4769
	Sayyad *et al.* (2018)	ESDBT	3.1635	3.8084	0.7764	2.5004	3.0979	0.5072
	Reddy (1984)	HSDBT	3.1654	3.8028	0.7305	2.5020	3.0916	0.4769
	Timoshenko (1921)	FSDBT	3.1657	3.7501	0.4922	2.5023	3.0396	0.3183
	Bernoulli-Euler (1744)	CBT	2.8783	3.7501	–	2.2693	3.0396	–
1	Present	ZSDBT	6.2594	5.8835	0.7329	4.9458	4.7856	0.4769
	Sayyad *et al.* (2018)	ESDBT	6.2563	5.8957	0.8288	4.9432	4.7964	0.5430
	Reddy (1984)	HSDBT	6.2594	5.8850	0.8031	4.9458	4.7856	0.5243
	Timoshenko (1921)	FSDBT	6.1790	5.7960	0.8313	4.8807	4.6979	0.3183
	Bernoulli-Euler (1744)	CBT	5.7746	5.7960	–	4.5528	4.6979	–
2	Present	ZSDBT	8.0677	6.8824	0.6704	6.3754	5.6004	0.4368
	Sayyad *et al.* (2018)	ESDBT	8.0666	6.8971	0.8485	6.3745	5.6149	0.5553
	Reddy (1984)	HSDBT	8.0677	6.8842	0.8446	6.3754	5.6004	0.5521
	Timoshenko (1921)	FSDBT	7.9253	6.7678	1.0791	6.2601	5.4856	0.2709
	Bernoulli-Euler (1744)	CBT	7.4003	6.7678	–	5.8346	5.4856	–
5	Present	ZSDBT	9.8281	8.1104	0.5904	7.7723	6.6057	0.3856
	Sayyad *et al.* (2018)	ESDBT	9.8414	8.1331	0.7654	7.7830	6.6281	0.5024
	Reddy (1984)	HSDBT	9.8281	8.1127	0.8114	7.7723	6.6057	0.5314
	Timoshenko (1921)	FSDBT	9.4987	7.9430	1.5373	7.5056	6.4382	0.2085
	Bernoulli-Euler (1744)	CBT	8.7508	7.9430	–	6.8994	6.4382	–
10	Present	ZSDBT	10.9381	9.7119	0.6465	8.6530	7.9080	0.4224
	Sayyad *et al.* (2018)	ESDBT	10.940	9.7345	0.6947	8.6547	7.9300	0.4560
	Reddy (1984)	HSDBT	10.938	9.7141	0.6448	8.6530	7.9080	0.4224
	Timoshenko (1921)	FSDBT	10.534	9.5231	1.9050	8.3259	7.7189	1.2320
	Bernoulli-Euler (1744)	CBT	9.6072	9.5231	–	7.5746	7.7189	–
∞	Present	ZSDBT	17.183	3.8019	0.7329	13.582	3.0916	0.4769
	Sayyad *et al.* (2018)	ESDBT	17.173	3.8084	0.7741	13.574	3.0980	0.5072
	Reddy (1984)	HSDBT	17.183	3.8028	0.7305	13.582	3.0916	0.4769
	Timoshenko (1921)	FSDBT	15.912	3.7501	0.4922	12.552	3.0396	0.3183
	Bernoulli-Euler (1744)	CBT	15.625	3.7501	–	12.319	3.0396	–

ESDBT of Sayyad (2018), HSDT of Reddy (1984), FSDT of Timoshenko (1921) and CBT of Bernoulli-Euler (1744) are specially generated. It is observed from Table 2 that the value of the transverse displacement is maximum when p=∞ whereas it is minimum when p=0. This is due to the fact that an increase of the power law index increases the flexibility of FG beams. The classical beam theory CBT shows low values of displacements as compared to other theories due to the fact that transverse shear deformation is neglected. Figs. 5 and 6 show the variation of axial displacement along the length and across the depth of the beam, respectively. It is pointed out from both the figures that the axial displacement is maximum when the beam is of full metal and minimum when the beam is of full

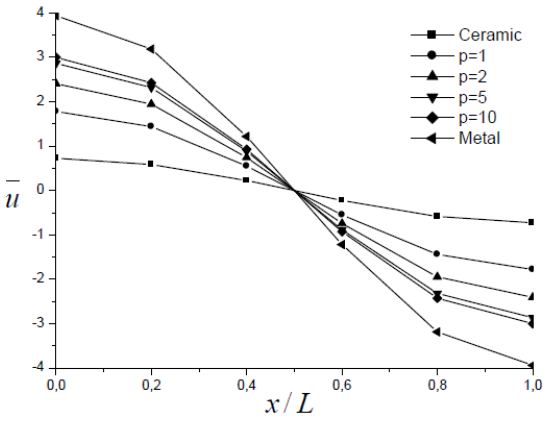

Fig. 5 Variation of non-dimensional axial displacement $\bar{u}$ along the length for simply supported functionally graded (P-FGM) beam subjected to sinusoidal load (L/h=5)

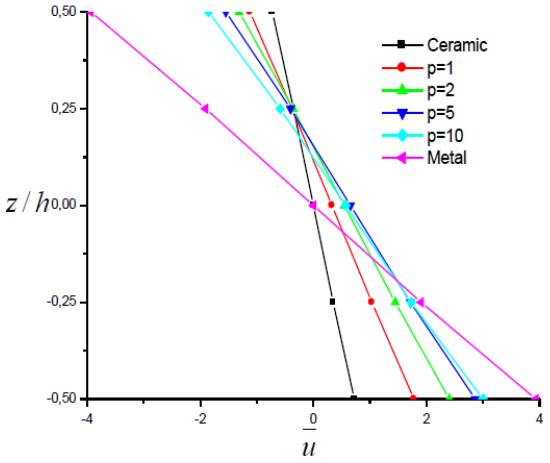

Fig. 6 The variation of the axial displacement $\bar{u}$ through-the-thickness for simply supported functionally graded (P-FGM) beam subjected to sinusoidal load (L/h=5)

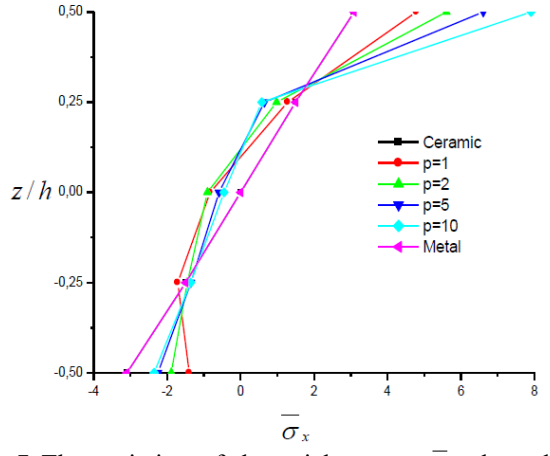

Fig. 7 The variation of the axial stress $\bar{\sigma}_x$ through-the-thickness for simply supported functionally graded (P-FGM) beam subjected to sinusoidal load (L/h=5)

ceramic. Due to varying properties through the thickness, the axial stress for FG beam is not zero at the neutral axis. It is also observed that the axial and shear stresses for fully

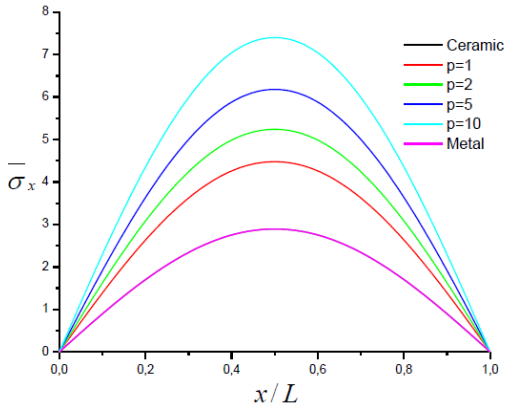

Fig. 8 The variation of the transverse displacement $\bar{\sigma}_x$ versus non-dimensional length of simply supported functionally graded (P-FGM) beam subjected to sinusoidal load (L/h=5)

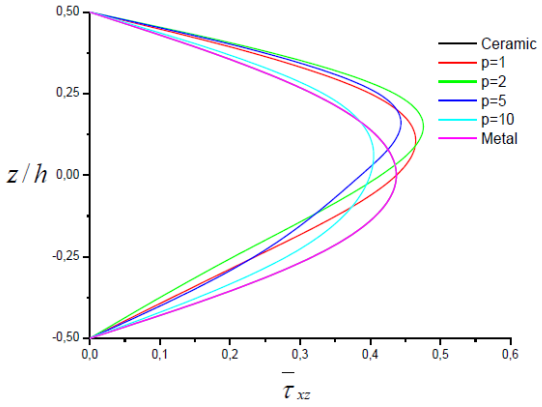

Fig. 9 The variation of the transverse shear stress $\bar{\tau}_{xz}$ through-the-thickness of simply supported functionally graded (P-FGM) beam subjected to sinusoidal load (L/h=5)

aluminum (p=∞) and fully alumina (p=0) beams are the same. Figs. 7 and 8 show the variation of axial stress along the length and depth of the beam. The variation of axial stress is non-linear when p=1, 2, 5, and 10, whereas linear for p=0 and ∞. The axial stress $\bar{\sigma}_x$ is tensile at the top surface and compressive at the bottom surface.

Fig. 9 shows that the present theory gives parabolic distribution of transverse shear stress across the depth and satisfies the zero shear stress conditions at top and bottom surfaces of the beam. The shear stresses of the full metal and the full ceramic beams coincide with each other.

Study 2 Effect of micromechanical models on bending analysis of FG beams using a new higher order shear deformation model.

The effect of micromechanical models on bending analysis of FG beams using a new higher order shear deformation model is presented for investigation. The example is performed in Table 3 for FG beam with power law index p=2 and L=5h. Effective Young's modulus is calculated using the aforementioned five micromechanical models. The results are given in terms of displacements and the various stresses. It can be observed that there is a good agreement between displacements and stresses using the

Table 3 Non-dimensional displacements and stresses of functionally graded (P-FGM) beams (p=2 and L=5h)

Theory		Uniform load				Sinusoidal load			
		$\bar{u}$	$\bar{w}$	$\bar{\sigma}_x$	$\bar{\tau}_{xz}$	$\bar{u}$	$\bar{w}$	$\bar{\sigma}_x$	$\bar{\tau}_{xz}$
Present	Voigt	3.1129	8.0677	6.8824	0.6704	2.4047	6.3754	5.6004	0.4368
	Reuss	3.7106	10.1403	8.9372	0.6481	2.8647	8.0184	7.2756	0.4231
	LRVE	3.5386	9.3292	7.8585	0.6290	2.7326	7.3756	6.3981	0.4104
	Tamura (q=0)	3.7106	10.1403	8.9372	0.6481	2.8647	8.0184	7.2756	0.4231
	Tamura (q=100)	3.5073	9.2981	7.9333	0.6414	2.7089	7.3504	6.4583	0.4184
	Mori-Tanaka	3.6480	9.8633	8.5824	0.6445	2.8166	7.7989	6.9869	0.4206

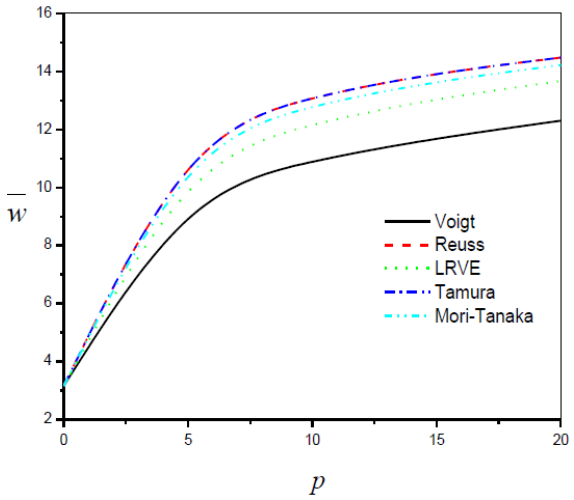

Fig. 10 The transverse displacement $\bar{w}$ versus the power law index p of FG beams for different micromechanical models (L/h=5)

different micromechanical models under uniform and sinusoidal loads. The slight difference may be explained by the way that the Young's modulus is calculated. In addition, the use of the Reuss model leads to the highest displacement values, compared to other models, while that of Voigt's one implies the lowest values. The LRVE and Tamura models lead to almost the same results.

In Fig. 10, the variations of the displacement $\bar{w}$ through the thickness direction of FG beam with the power law index p are given for different micromechanical models. It is seen from the figure that the increase of the power law index p produces an increase in the values of the displacement and this whatever the model used. In addition, the Reuss model has the highest displacement values compared to other models. While that of Voigt has the lowest values. The Tamura and Reuss models have the practically same results.

Study 3 Bending analysis of simply supported imperfect and perfect FG beams.

In order to explicitly understand the porosity effect on the bending behavior of FG beams, Fig. 11 shows variations of the nondimensional axial normal stress $\bar{\sigma}_x$ of FG perfect and imperfect beams across the depth under uniform load at a constant value of span-to-depth ratio (L/h=5). From this figure, it can be concluded that the influence of

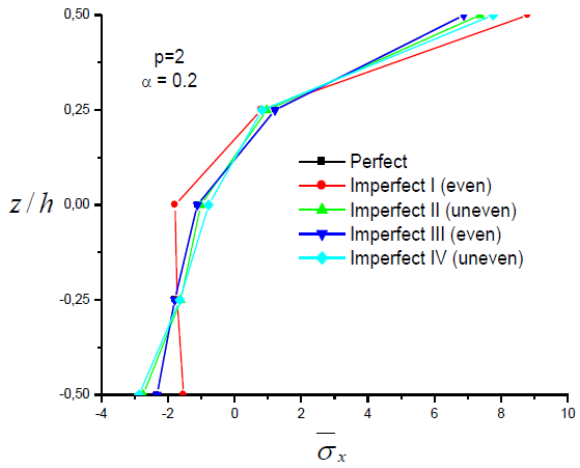

Fig. 11 Variation of nondimensional axial normal stress $\bar{\sigma}_x(l/2, z)$ of embedded perfect and imperfect FG beams across the depth under uniform load (p=2, α=0.2)

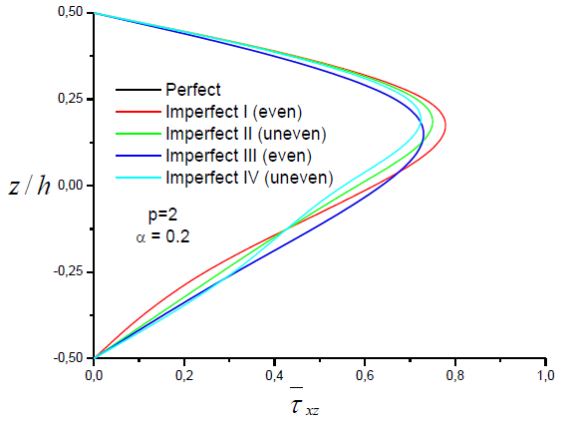

Fig. 12 Variation of nondimensional transverse shear stress $\bar{\tau}_{xz}(0, z)$ of embedded perfect and imperfect FG beams across the depth of FG beams under uniform m load (p=2, α=0.2

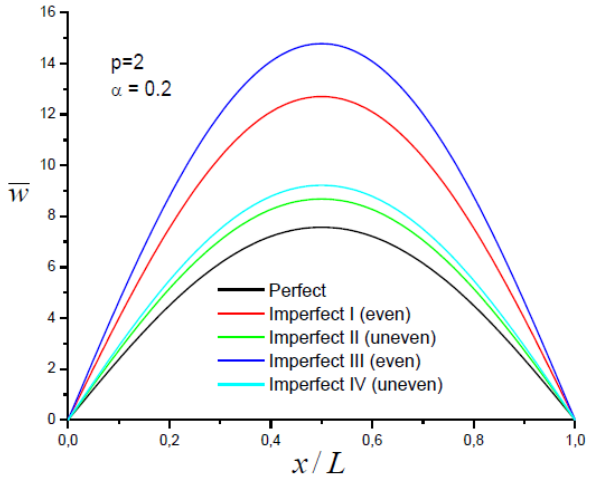

Fig. 13 The variation of the transverse displacement $\bar{w}$ of embedded perfect and imperfect FG beams versus non-dimensional length beam subjected to uniform load (L/h=5)

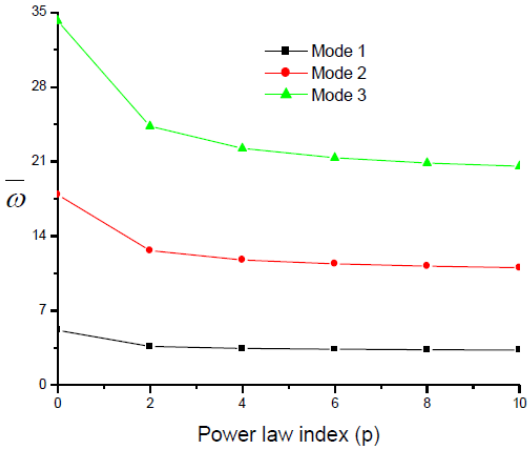

Fig. 14 Variation of non-dimensional flexural natural frequencies $\bar{\omega}$ of simply supported functionally graded (P-FGM) beam with respect to power law index (L/h=5)

the porosity on the bending of imperfect beams with even porosities distribution (Imperfect I and III) and uneven porosities distribution (Imperfect II and IV) is very clear. The stresses are tensile at the top surface and compressive at the bottom surface and take the maximum and the minimum values for the even porosities distribution (Imperfect I) respectively. In addition, the even porosities distribution (Imperfect III), and the perfect beam have practically almost the same results.

Fig. 12 shows the distribution of the shear stresses of embedded perfect and imperfect FG beams across the depth under uniform load. The volume fraction exponent of the FG beam in taken as p=2. It is clear that the distributions are not parabolic and the stresses increase for the imperfect FG beam. The even porosities distribution (Imperfect I) gives the highest value of shear stress compared to other distributions of porosity. Also, the even porosities distribution (Imperfect III), and the perfect beam have almost the same results.

Fig. 13 illustrates the variation of the non-dimensional transversal displacement of perfect and imperfect FG beams versus non-dimensional length beam subjected to uniform load (L/h=5). The deflection is maximum for the even porosities distribution (Imperfect III), and minimum for the perfect FG beam (α=0).

Study 4 Free vibration analysis of simply supported functionally graded (P-FGM) beams.

The first three non-dimensional flexural natural frequencies $\bar{\omega}$ of FG beams for different values of power law index p and span-to-depth ratio L/h are compared to the corresponding results presented by Simsek (2010), Vo *et al.* (2014b), Timoshenko (1921), using the first-order beam theories, Reddy (1984), Simsek (2010), Thai and Vo (2012), Vo *et al.* (2014b) using the higher order beam theories, Sayyad *et al.* (2018) using the exponential higher order beam theories and classical beam theory of Bernoulli-Euler (1744) in Table 4. The examination of Table 4 reveals that the present flexural natural frequencies are in good agreement with those presented by other researchers. It is pointed out that the natural frequencies decrease with the increase of the power law index p and increase with

Table 4 Non-dimensional flexural natural frequencies ($\bar{\omega}$) of simply supported functionally graded (P-FGM) beams

L/h	Mode	Theory	Model	Power law index (p)					
				0 (ceramic)	1	2	5	10	∞ (Metal)
5	1	Present	ZSDBT	5.15274	3.99042	3.62643	3.40120	3.28160	2.67732
		Sayyad *et al.* (2018)	ESDBT	5.15423	3.99140	3.62671	3.40000	3.28135	2.67810
		Reddy (1984)	HSDBT	5.15274	3.99042	3.62643	3.40120	3.28160	2.67732
		Simsek (2010)	FSDBT	5.15247	3.99023	3.63438	3.43119	3.31343	2.67718
		Simsek (2010)	HSDBT	5.15274	3.99042	3.62643	3.40120	3.28160	2.67732
		Thai and Vo (2012)	HSDBT	5.15275	3.99042	3.62644	3.40120	3.28160	2.67732
		Vo *et al.* (2014b)	FSDBT	5.15260	3.97108	3.60495	3.40253	3.29625	2.67725
		Vo *et al.* (2014b)	HSDBT	5.15275	3.97160	3.59791	3.37429	3.26534	2.67732
		Timoshenko (1921)	FSDBT	5.15247	3.99023	3.63438	3.43119	3.31343	2.67718
		Bernoulli-Euler (1744)	CBT	5.39530	4.14840	3.77930	3.59490	3.49210	2.80336
	2	Present	ZSDBT	17.8812	14.0099	12.6405	11.5431	11.0240	9.2909
		Sayyad *et al.* (2018)	ESDBT	17.8996	14.0224	12.6466	11.5281	11.0264	9.03573
		Thai and Vo (2012)	HSDBT	17.8810	14.0098	12.6407	11.5444	11.0246	–
		Bernoulli-Euler (1744)	CBT	20.6187	15.7982	14.3260	13.5876	13.2376	–
	3	Present	ZSDBT	34.2097	27.0979	24.3151	21.7158	20.5561	17.7750
		Sayyad *et al.* (2018)	ESDBT	33.3835	27.2496	24.6889	21.3661	20.5815	17.3457
		Thai and Vo (2012)	HSDBT	34.2085	27.0971	24.3151	21.7187	20.5569	–
		Bernoulli-Euler (1744)	CBT	43.3483	33.0278	29.7458	28.0850	27.4752	–
20	1	Present	ZSDBT	5.46032	4.20505	3.83613	3.64849	3.53898	2.83714
		Sayyad *et al.* (2018)	ESDBT	5.46043	4.20513	3.83614	3.64830	3.53895	2.83720
		Reddy (1984)	HSDBT	5.46030	4.20503	3.83611	3.64850	3.53896	2.83716
		Simsek (2010)	FSDBT	5.46032	4.20505	3.83676	3.65088	3.54156	2.83713
		Simsek (2010)	HSDBT	5.46030	4.20503	3.83611	3.64850	3.53896	2.83716
		Thai and Vo (2012)	HSDBT	5.46032	4.20505	3.83613	3.64849	3.53899	2.83714
		Vo *et al.* (2014b)	FSDBT	5.46033	4.20387	3.83491	3.64903	3.54045	2.83714
		Vo *et al.* (2014b)	HSDBT	5.46032	4.20387	3.83428	3.64663	3.53787	2.83714
		Timoshenko (1921)	FSDBT	5.46032	4.20505	3.83676	3.65088	3.54156	2.83713
		Bernoulli-Euler (1744)	CBT	5.47770	4.21630	3.84720	3.66280	3.55470	2.84618
	2	Present	ZSDBT	21.5732	16.6344	15.1619	14.3746	13.9263	11.2093
		Sayyad *et al.* (2018)	ESDBT	21.5738	16.6342	15.1620	14.3670	13.9147	11.2096
		Thai and Vo (2012)	HSDBT	21.5732	16.6344	15.1619	14.3748	13.9264	–
		Bernoulli-Euler (1744)	CBT	21.8438	16.8100	15.3334	14.5959	14.1676	–
	3	Present	ZSDBT	47.5929	36.7679	33.4689	31.5780	30.5369	24.7289
		Sayyad *et al.* (2018)	ESDBT	47.5913	36.8705	33.6304	31.5655	30.5349	27.5383
		Thai and Vo (2012)	HSDBT	47.5930	36.7679	33.4691	31.5789	30.5373	–
		Bernoulli-Euler (1744)	CBT	48.8999	37.6173	34.2954	32.6357	31.6883	–

Table 5 Variation of frequency parameters $\bar{\omega}$ of perfect and imperfect FG beam (p=2)

L/h	Perfect	Imperfect I (even)		Imperfect II (uneven)		Imperfect III (even)		Imperfect IV (uneven)		Imperfect V (logarithmic-uneven)	
	α=0	α=0.1	α=0.2	α=0.1	α=0.2	α=0.1	α=0.2	α=0.1	α=0.2	α=0.1	α=0.2
5	3.6264	3.4418	3.1489	3.6069	3.5785	3.6264	3.6264	3.7167	3.8055	3.6075	3.5816
20	3.8361	3.6335	3.3123	3.8226	3.8004	3.8361	3.831	3.9527	4.0725	3.8230	3.8029

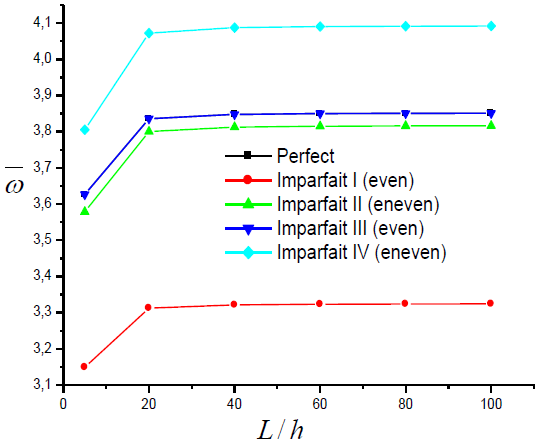

Fig. 15 Variation of the fundamental frequency $\bar{\omega}$ of embedded perfect and imperfect FG beams (p=2) versus L/h ratio (α=0.2)

increasing mode number. This is due to the fact that an increase of the power law index p makes FG beams more flexible. The same remarks are noted in Fig. 14.

Study 5 Free vibration analysis of embedded perfect and imperfect FG beams.

Table 5 shows the variations of the nondimensional frequency of FG perfect and imperfect beams at a constant value of power law index (p=2) for two values of porosity volume fraction α. It can be concluded that the influence of the porosity on the frequency of imperfect beams with even porosities distribution (Imperfect I and III), and uneven porosities distributions (Imperfect II and IV) is very clear. The even porosities distributions (Imperfect III), and the perfect beam have almost the same frequencies. The difference between the results calculated with the four models of porosities, are slightly different. This can be explained by the way who the Young's modulus is calculated. Fig. 15 illustrates the variation of the fundamental frequency $\bar{\omega}$ of embedded perfect and imperfect FG beams versus L/h ratio with α=0.2. It can be also seen that the span-to-depth ratio L/h has a considerable effect on the non-dimensional fundamental natural frequency $\bar{\omega}$ where this latter is reduced with decreasing L/h. This dependence is related to the effect of shear deformation.

5. Conclusions

Bending and free vibration analysis of perfect and imperfect FG beams under uniform and sinusoidal loads is carried out in the present study by a new higher order shear deformation model. The theory accounts for higher-order variation of transverse shear strain through the depth of the beam and satisfies the zero traction boundary conditions on the surfaces of the beam without using shear correction factors. Different patterns of porosity distributions (including even and uneven distribution patterns, and the logarithmic-uneven pattern) are considered. In addition, the effect of different micromechanical models on the bending

and free vibration response of these beams is studied. Various micromechanical models are used to evaluate the mechanical characteristics of the FG beams for which properties vary continuously across the thickness according to a simple power law. The results generated in the present work for various analyses are compared with the existing published results. The comparison proves the accuracy of the presently considered shear deformation theory, and hence it can successfully be employed for the structural analyses of FG beams.

References

Ait Amar Meziane, M., Abdelaziz, H.H. and Tounsi, A. (2014), "An efficient and simple refined theory for buckling and free vibration of exponentially graded sandwich plates under various boundary conditions", *J. Sandw. Struct. Mater.*, **16**(3), 293-318.

Akbarzadeh, A.H., Abedini, A. and Chen, Z.T. (2015), "Effect of micromechanical models on structural responses of functionally graded plates", *Compos. Struct.*, **119**, 598-609.

Akbaş, S.D. (2015a), "Wave propagation of a functionally graded beam in thermal environments", *Steel Compos. Struct.*, **19**(6), 1421-1447.

Akbaş, S.D. (2015b), "On post-buckling behavior of edge cracked functionally graded beams under axial loads", *Int. J. Struct. Stab. Dyn.*, **15**(4), 1450065.

Akbaş, S.D. (2015c), "Post-buckling analysis of axially functionally graded three-dimensional beams", *Int. J. Appl. Mech.*, **7**(3), 1550047.

Akbaş, S.D. (2017a), "Nonlinear static analysis of functionally graded porous beams under thermal effect", *Coupled Syst. Mech.*, **6**(4), 399-415.

Akbaş, S.D. (2017b), "Post-buckling responses of functionally graded beams with porosities", *Steel Compos. Struct.*, **24**(5), 579-589.

Akbaş, S.D. (2017c), "Thermal effects on the vibration of functionally graded deep beams with porosity", *Int. J. Appl. Mech.*, **9**(5), 1750076.

Akbaş, S.D. (2017d), "Vibration and static analysis of functionally graded porous plates", *J. Appl. Comput. Mech.*, **3**(3), 199-207.

Akbaş, S.D. (2018a), "Forced vibration analysis of functionally graded porous deep beams", *Compos. Struct.*, **186**, 293-302.

Akbaş, S.D. (2018b), "Geometrically nonlinear analysis of functionally graded porous beams", *Wind Struct.*, **27**(1), 59-70.

Atmane, H.A., Tounsi, A., Bernard, F. and Mahmoud, S.R. (2015), "A computational shear displacement model for vibrational analysis of functionally graded beams with porosities", *Steel Compos. Struct.*, **19**(2), 369-384.

Belabed, Z., Houari, M.S.A., Tounsi, A., Mahmoud, S.R. and Anwar Bég, O. (2014), "An efficient and simple higher order shear and normal deformation theory for functionally graded material (FGM) plates", *Compos.: Part B*, **60**, 274-283.

Bouiadjra, R.B., Mahmoudi, A., Benyoucef, S., Tounsi, A. and Bernard, F. (2018), "Analytical investigation of bending response of FGM plate using a new quasi 3D shear deformation theory: Effect of the micromechanical models", *Struct. Eng. Mech.*, **66**(3), 317-328.

Euler, L. (1744), *Methodus Inveniendi Lineas Curvas Maximi Minimive Proprietate Gaudentes, Lausanne and Geneva: Apud Marcum-Michaelem Bousquet & Socio*, 1-322.

Gasik, M. (1995), "Scand. Ch226", *Acta Polytech*, **72**.

Gasik, M.M. (1998), "Micromechanical modeling of functionally graded materials", *Comput. Mater. Sci.*, **13**, 42-55.

Gupta, A. and Talha, M. (2017), "Influence of porosity on the flexural and free vibration responses of functionally graded plates in thermal environment", *Int. J. Struct. Stab. Dyn.*, **18**(1), 1850013.

Hamidi, A., Houari, M.S.A., Mahmoud, S.R. and Tounsi, A. (2015), "A sinusoidal plate theory with 5-unknowns and stretching effect for thermomechanical bending of functionally graded sandwich plates", *Steel Compos. Struct.*, **18**(1), 235-253.

Hebali, H., Tounsi, A., Houari, M.S.A., Bessaim, A. and Adda Bedia, E.A. (2014), "A new quasi-3D hyperbolic shear deformation theory for the static and free vibration analysis of functionally graded plates", *ASCE J. Eng. Mech.*, **140**(2), 374-383.

Jaesang, Y. and Addis, K. (2014), "Modeling functionally graded materials containing multiple heterogeneities", *Acta Mech.*, **225**(7), 1931-1943.

Jha, D.K., Kant, T. and Singh, R.K. (2013), "Critical review of recent research on functionally graded plates", *Compos. Struct.*, **96**, 833-849.

Ju, J. and Chen, T.M. (1994), "Micromechanics and effective moduli of elastic composites containing randomly dispersed ellipsoidal inhomogeneities", *Acta Mech.*, **103**(1-4), 103-121.

Kendall, K., Howard, A., Birchall, J., Prat, P., Proctor, A. and Jefferies, S.A. (1983), "The relation between porosity, microstructure and strength, and the approach to advanced cement-based materials", *Phil. Trans. Roy. Soc. Lond. A*, **310**(1511), 139-153.

Kitipornchai, S., Yang, J. and Liew, K.M. (2006), "Random vibration of the functionally graded laminates in thermal environments", *Comp. Meth. Appl. Mech. Eng.*, **195**(9-12), 1075-1095.

Mahi, A., Adda Bedia, E.A. and Tounsi, A. (2015), "A new hyperbolic shear deformation theory for bending and free vibration analysis of isotropic, functionally graded, sandwich and laminated composite plates", *Appl. Math. Modell.*, **39**(9), 2489-2508.

Mishnaevsky, J.L. (2007), *Computational Mesomechanics of Composites*, John Wiley & Sons, U.K.

Reddy, J.N. (1984), "A simple higher order theory for laminated composite plates", *ASME J. Appl. Mech.*, **51**(4), 745-752.

Sayyad, A.S. and Ghugal, Y.M. (2018), "Analytical solutions for bending, buckling, and vibration analyses of exponential functionally graded higher order beams", *Asian J. Civil Eng.*, 1-17.

Shen, H.S. and Wang, Z.X. (2012), "Assessment of Voigt and Mori-Tanaka models for vibration analysis of functionally graded plates", *Compos. Struct.*, **94**(7), 2197-2208.

Timoshenko, S.P. (1921), "On the correction for shear of the differential equation for transverse vibrations of prismatic bars", *Philosoph. Mag.*, **41**(245), 742-746.

Wang, Y.Q. and Zu, J.W. (2017), "Vibration behaviors of functionally graded rectangular plates with porosities and moving in thermal environment", *Aerosp. Sci. Technol.*, **69**, 550-562.

Wattanasakulpong, N. and Ungbhakorn, V. (2014), "Linear and nonlinear vibration analysis of elastically restrained ends FGM beams with porosities", *Aerosp. Sci. Technol.*, **32**(1), 111-120.

Yin, H.M., Paulino, G.H., Buttlar, W.G. and Sun, L.Z. (2007), "Micromechanics-based thermoelastic model for functionally graded particulate materials with particle interactions", *J. Mech. Phys. Sol.*, **55**(1), 132-160.

Zhu, J., Lai, Z., Yin, Z., Jeon, J. and Lee, S. (2001), "Fabrication of ZrO_2-NiCr functionally graded material by powder metallurgy", *Mater. Chem. Phys.*, **68**(1-3), 130-135.

CC